# An Improved Mathematical Model of Lead-Acid Batteries for Simulation of VRLA Batteries

**Vahid Esfahanian**
Associated Professor
evahid@ut.ac.ir

**Farschad Torabi**
Ph. D. Candidate
ftorabi@ut.ac.ir

**Ali Mosahebi**
M.Sc Student
amosahebi@ut.ac.ir

Vehicle, Fuel and Environment Research Institute

Faculty of Mechanical Engineering

College of Engineering – University of Tehran

## Abstract

Predicting transient behavior of lead-acid batteries during charge and discharge process is an important factor in many applications including Hybrid Electric Vehicles (HEV) where side reactions like oxygen recycle and hydrogen evolution are present in battery. In this study, an improved mathematical model for VRLA batteries based on Computational Fluid Dynamics (CFD) and Equivalent Circuit Model (ECM) has been introduced. This model inherits accuracy of CFD model and physical understanding of ECM. Moreover, it is very fast which makes it quite suitable for real-time simulations. The present approach is verified by previous CFD models and experimental data.

## 1. Introduction

Lead-acid batteries are widely perceived as the best near-term power source for electric vehicles (EV) due to their low cost, versatility, and excellent rechargeability and recyclability. Important characteristics of EV batteries include high specific energy and energy density, high specific power and power density, and long cycle life. A long cycle life is a key requirement if advanced EV batteries are to have reasonable life cycle costs. In order to predict and further improve these characteristics, it is important to understand the dynamic behavior of EV lead-acid batteries during charge, rest and discharge cycles. To complement the conventional trial-and-error method of improving the performance and cycle life of the lead-acid battery, mathematical models have been developed to predict discharge and charge behavior, as well as the effect of cycling.

Newman and Tiedmann first developed a comprehensive porous electrode theory and applied it to simulate the discharge behavior of a lead-acid cell [1]. Bernardi et al. proposed a two-dimensional model to simulate the effects of the current collector tabs [2]. Most recently C.Y. Wang and W.B. Gu developed the mathematical governing equations of batteries which are obtained from the conservation laws [3]. In their model, the effect of free convection has been considered and it was shown that fluid dynamics have a very important role in the batteries dynamic behavior. These equations can be used in all kinds of batteries (VRLA or Vented lead-acid batteries) with little modification.

Computational fluid dynamics (CFD) can be used to solve these governing equations of battery dynamics to obtain an insightful understanding of battery performance and detailed characteristics of its behavior. W. B. Gu et al. used CFD techniques and numerically solved the governing equations of VRLA batteries [4]. Esfahanian and Torabi [5] solved these governing equations using
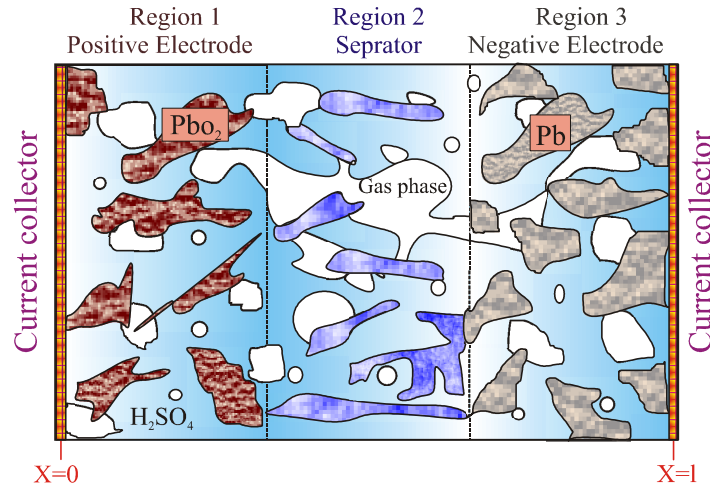
Figure 1: Schematic illustration of a lead-acid cell.

Keller-Box method and investigated the effect of acid concentration dependency of open circuit voltage on battery behavior.
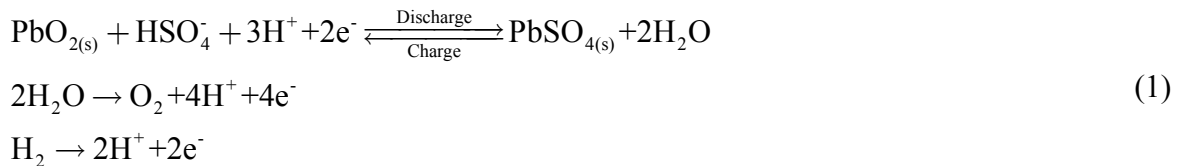
Since the governing equations of battery dynamics are mathematically nonlinear and stiff, the solution of the system requires many iterations which makes it time consuming. Therefore, CFD models are normally used for design purposes and are not suitable for real time applications.

Other simulation methods such as equivalent circuit model (ECM) [6] and engineering methods [7] are fast enough for real-time applications but the former suffers from lack of accuracy and the engineering method does not provide any insightful information about the battery.
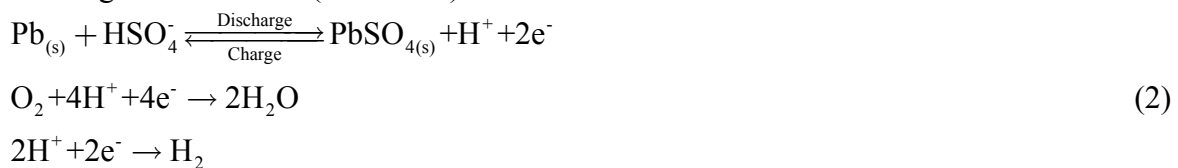
To overcome the above mentioned problems of previous models, a new mathematical model is developed which is a combination of CFD and ECM. The new developed modeling inherits accuracy of CFD models and physical understanding of ECM. Moreover, it is fast enough for real-time simulations. The present approach is verified by previous CFD models and experimental data.

## 2. Mathematical Model

A typical lead-acid cell is shown schematically in Figure 1 which consists of the following regions: a lead-grid collector at x=0 which is at the center of the positive electrode; a positive $PbO_2$ electrode; a porous separator; a negative Pb electrode; and finally, a lead-grid collector at x=l which is at the center of the negative electrode. The positive and negative electrodes consist of porous solid matrices whose pores are flooded by a binary sulfuric acid, $H_2SO_4$, and the gaseous phase that is consisted of $O_2$, $H_2$ and $N_2$. During charge and discharge, the following electrochemical reactions occur in the positive electrode ($PbO_2/PbSO_4$):

$$PbO_{2(s)} + HSO_4^- + 3H^+ + 2e^- \underset{Charge}{\overset{Discharge}{\rightleftharpoons}} PbSO_{4(s)} + 2H_2O$$

$$2H_2O \rightarrow O_2 + 4H^+ + 4e^- \tag{1}$$

$$H_2 \rightarrow 2H^+ + 2e^-$$

and the negative electrode ($Pb/PbSO_4$):

$$Pb_{(s)} + HSO_4^- \underset{Charge}{\overset{Discharge}{\rightleftharpoons}} PbSO_{4(s)} + H^+ + 2e^-$$

$$O_2 + 4H^+ + 4e^- \rightarrow 2H_2O \tag{2}$$

$$2H^+ + 2e^- \rightarrow H_2$$

The side reactions constitute the internal oxygen and hydrogen cycles in the cell. In the presence of side reactions, a VRLA cell is a three-phase system consisting of the solid matrix, the liquid electrolyte and a gas phase. During charging and over charging, the oxygen is generated at the PbO$_2$ electrolyte interface and may evolve into the gas phase after exceeding its solubility limit in the electrolyte.

The oxygen can then be transported, via the liquid and gas phase, from the positive to the negative electrode where the oxygen gas may dissolve back in the electrolyte and be reduced at the Pb electrode interface. This process forms an internal oxygen cycle in VRLA cells.

Table 1: Summary of governing equations

| | | |
|---|---|---|
| Kinetic rate Equations $\eta_j = \phi_s - \phi_e - U_j$ | • Primary reactions ($j$=1 and 4): | $i_{nj} = i_{0j,\text{ref}} \left(\dfrac{c^H}{c_{\text{ref}}^H}\right)^{\gamma} \left[\exp\left(\dfrac{\alpha_{aj}F}{RT}\eta_j\right) - \exp\left(\dfrac{-\alpha_{cj}F}{RT}\eta_j\right)\right]$ |
| | • Oxygen generation recombination ($j$=2 and 5): | |
| | | $i_{nj} = i_{0j,\text{ref}} \left(\dfrac{c^H}{c_{\text{ref}}^H}\right)^{\gamma_{O_2}} \left[\exp\left(\dfrac{\alpha_{aj}F}{RT}\eta_j\right) - \left(\dfrac{c_e^{O_2}}{c_{e,\text{ref}}^{O_2}}\right)^{\delta_{O_2}} \exp\left(\dfrac{-\alpha_{cj}F}{RT}\eta_j\right)\right]$ |
| | • Hydrogen evolution ($j$=6): | $i_{nj} = -i_{0j,\text{ref}} \left(\dfrac{c^H}{c_{\text{ref}}^H}\right)^{\gamma_{H_2}} \exp\left(\dfrac{-\alpha_{cj}F}{RT}\eta_j\right)$ |
| Conservation of Charge | • In electrolyte: | $\nabla.(k^{\text{eff}}\nabla\phi_e) + \nabla.[k_D^{\text{eff}}\nabla(\ln c^H)] + S_e^c = 0$ |
| | • In solid electrode: | $\nabla.(\sigma^{\text{eff}}\nabla\phi_s) - S_e^c = 0$ |
| Conservation of Species | • In electrolyte: | $\dfrac{\partial(\varepsilon_e c^H)}{\partial t} = \nabla.(D_{\text{eff}}^H \nabla c^H) + S^H$ |
| | | $\dfrac{\partial(\varepsilon_e c_e^{O_2})}{\partial t} = \nabla.(D_{e,\text{eff}}^{O_2}\nabla c_e^{O_2}) + S_e^{O_2}$ |
| | • In gas phase: | $\dfrac{\partial(\varepsilon_g c_g^{O_2})}{\partial t} = \nabla.(D_{g,\text{eff}}^{O_2}\nabla c_g^{O_2}) + J_{eg}^{O_2}$ |
| Conservation of Mass | • In electrolyte: | $\dfrac{\partial\varepsilon_e}{\partial t} = S_e^V$ |
| | • In solid electrode: | $\dfrac{\partial\varepsilon_s}{\partial t} = S_s^V$ |

Table 2: Source terms in conservation equations

| Terms | Positive Electrode | Separator | Negative Electrode |
|---|---|---|---|
| $S_e^c$ | $a_1 i_{n1} + a_2 i_{n2}$ | $0$ | $a_4 i_{n4} + a_5 i_{n5} + a_6 i_{n6}$ |
| $S^H$ | $\dfrac{3-2t_+^0}{2F}a_1 i_{n1} + \dfrac{1-t_+^0}{F}a_2 i_{n2}$ | $0$ | $\dfrac{1-2t_+^0}{2F}a_4 i_{n4} + \dfrac{1-t_+^0}{F}(a_5 i_{n5} + a_6 i_{n6})$ |
| $S_e^{O_2}$ | $\dfrac{1}{4F}a_2 i_{n2} - J_{eg}^{O_2}$ | $-J_{eg}^{O_2}$ | $\dfrac{1}{4F}a_5 i_{n5} - J_{eg}^{O_2}$ |
| $J_{eg}^{O_2}$ | $k(c_e^{O_2} - H'c_g^{O_2}),\ k = a_{eg}\dfrac{D_e^{O_2}}{l_{eg}}$ | | |
| $S_e^V$ | $\left[\bar{V}_e(3-2t_+^0) - 2\bar{V}_o\right]\dfrac{a_1 i_{n1}}{2F} +$ $\left[\bar{V}_e(2-2t_+^0) - \bar{V}_o\right]\dfrac{a_2 i_{n2}}{2F}$ | $0$ | $\bar{V}_e(1-2t_+^0)\dfrac{a_4 i_{n4}}{2F} + \left[\bar{V}_e(2-2t_+^0) - \bar{V}_o\right]\dfrac{a_5 i_{n5}}{2F}$ $+ \left[\bar{V}_e(2-2t_+^0)\right]\dfrac{a_6 i_{n6}}{2F}$ |
| $S_s^V$ | $\left(\dfrac{M_{PbO_2}}{\rho_{PbO_2}} - \dfrac{M_{PbSO_4}}{\rho_{PbSO_4}}\right)\dfrac{a_1 i_{n1}}{2F}$ | $0$ | $\left(\dfrac{M_{PbSO_4}}{\rho_{PbSO_4}} - \dfrac{M_{Pb}}{\rho_{Pb}}\right)\dfrac{a_4 i_{n4}}{2F}$ |

Hydrogen recombination occurring at the positive electrode is negligible because of its poor kinetics. Accumulation of oxygen and hydrogen in the gas phase contributes to the cell pressure build-up, thereby causing venting.

General governing equations of battery dynamics have been developed by Wang and Gu [3] which includes all chemical and electrochemical reactions as well as the flow motion. Gu and Wang used these equations to simulate VRLA batteries [4]. In the present study, these equations are simplified for lead-acid batteries and summarized in Table 1, along with source terms listed in Table 2.
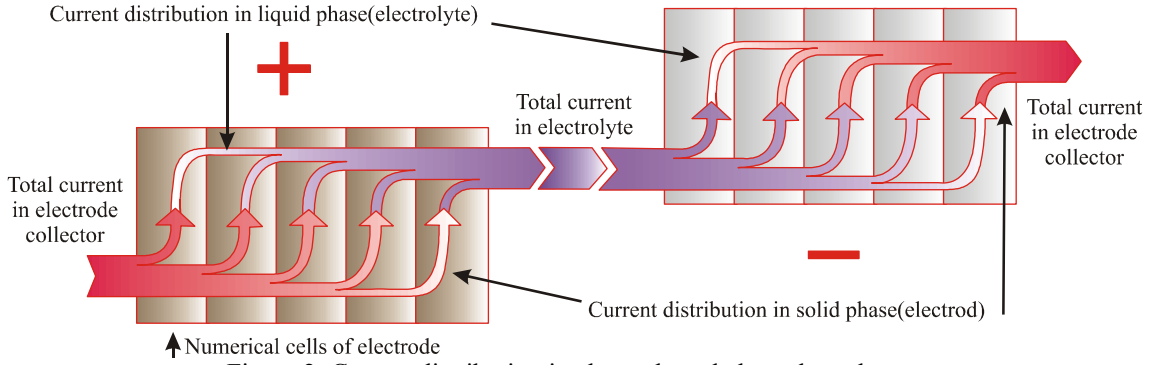


Figure 2: Current distribution in electrode and electrolyte phases.
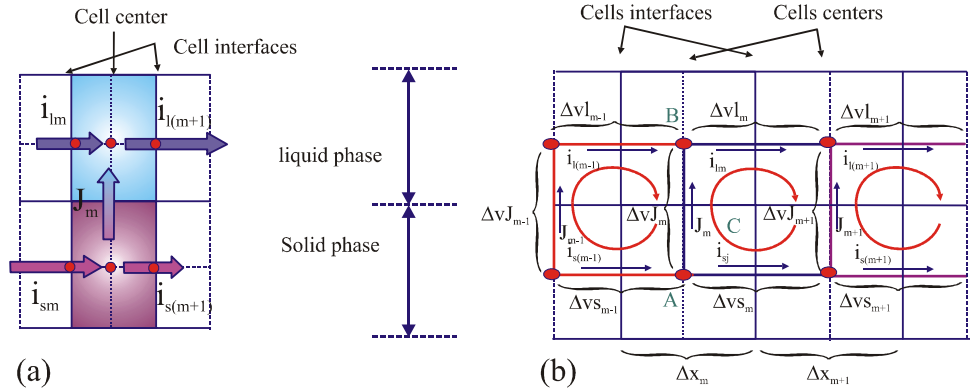


Figure 3: Schematic illustration of (a) computational volume and (b) volume circuit model.

In general, the applied current should be conserved throughout the cell. This current enters the cell from external circuit and enters the solid phase. As it can be seen schematically in Figure 2, the current enters the electrolyte through surface reactions whose rate is determined by kinetics of the reactions. At the end of solid phase, all the current enters the electrolyte phase through which is carried by ions to the other electrode. On the other electrode surface, this current enters the solid phase again in a reverse manner. In this model, the current in the gas phase is neglected.

To obtain the dynamic behavior of battery system, the governing system of coupled electrochemical equations should be solved numerically. In the present study, a two step scheme is introduced. In the first step, the conservation of charge equations are considered. Mathematically, these two couple equations have elliptic nature whose solution requires a lot of computational time. To reduce the computational time, these equations are combined by Kirchhoff's current and voltage laws (KCL and KVL) and are solved with an ECM based finite volume method.

Using this new form of discretization, the distribution of $\phi_s$ and $\phi_l$ can be obtained much faster than the previous works which were based on finite difference or finite volume methods [4-5]. Once the distribution of $\phi_s$ and $\phi_l$ is obtained (at each time level), in the second step, the equations of conservation of species are solved using Keller-Box method [5]. Since these equations are parabolic and as it can be seen in the governing equations, both functions and their derivatives are present.

Therefore, a suitable method to solve the problem numerically would be the Keller-Box method. These two steps are considered in more detail in the next section.

## 2.1. Step 1

To obtain the potential in solid and electrolyte and current transfer between these two phases, each electrode is divided into some control volumes in which all the parameters are assumed to be uniform. Each control volume can be modeled by an electric circuit which is shown in Figure 3(a). As it can be seen, on the junction of solid surface of the electrode and electrolyte, a voltage difference exists which is known as overpotential. The surface overpotential is the driven potential which causes the current enters the electrolyte. The amount of this current can be determined by kinetic equation which is known as Butler-Volmer equation. For main reactions (j=1,4 in Table 1) this equation is given as follow:

$$j = i_0 \left( \frac{c^H}{c_{ref}^H} \right)^{\gamma} \left\{ \exp\left( \frac{\alpha_a F}{RT} \eta \right) - \exp\left( -\frac{\alpha_c F}{RT} \eta \right) \right\} \tag{3}$$

For side reactions, this equation can be used with a little modification as given in Table 1.

The electro-neutrality indicates that the sum of the current that enters a control volume must leave, because no current is generated inside the volume. Using this fact and the KCL in the electric circuit shown in Figure 3(b), the conservation of current in node A becomes

$$i_{s(m-1)} - i_{s(m)} - J_m = 0 \tag{4}$$

and conservation of current in node C

$$i_{l(m-1)} - i_{l(m)} - J_m = 0 \tag{5}$$

also from KVL we have

$$(\phi_{s(m+1)} - \phi_{s(m)}) + (\phi_{l(m+1)} - \phi_{s(m+1)}) + (\phi_{l(m)} - \phi_{l(m+1)}) + (\phi_{s(m)} - \phi_{l(m)}) = 0 \tag{6}$$

in which $J_i = s_{ei} \Delta x_i$, and the currents in solid and electrolyte can be obtained from Ohm's law:

$$i_s = -\sigma \frac{\partial \phi_s}{\partial x} \tag{7}$$

and

$$i_l = -k \frac{\partial \phi_l}{\partial x} - k_D \frac{\partial}{\partial x} (\ln \ c) \tag{8}$$

Equations (6) and (7) can be discritized as follows:

$$i_{sm} = \frac{\Delta V s_m}{Rs_m^{eff}} \tag{9}$$

in which $Rs_m^{eff} = \frac{Rs_m + Rs_{(m+1)}}{2}$, and $Rs_m = \frac{\Delta x_m}{\sigma_m^{eff}}$. In the same manner we have
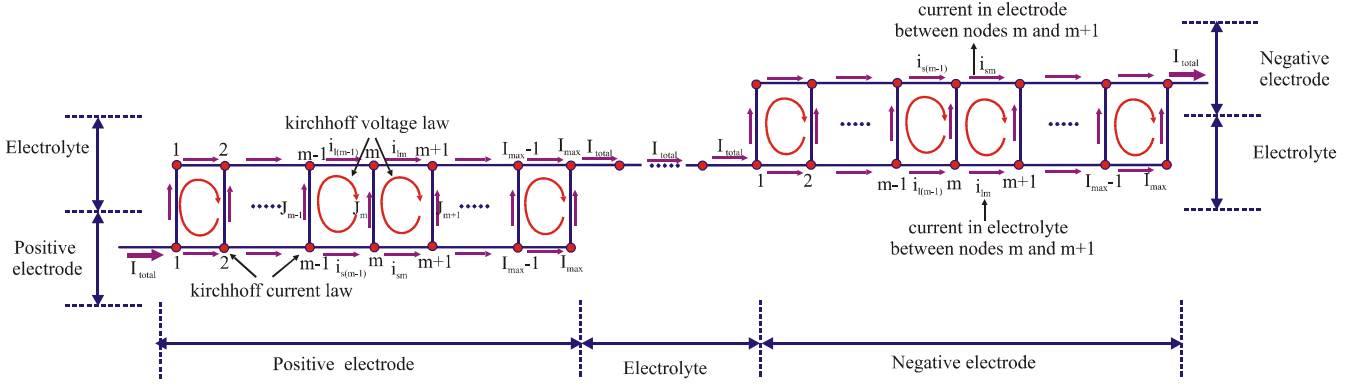
Figure 4: Equivalent Circuit Model of the whole battery cell.

$$i_{lm} = \frac{\Delta V l_m}{R l_m^{eff}} - k_D \frac{1}{c} \frac{\partial c}{\partial x} \tag{10}$$

in which $R l_m^{eff} = \frac{R l_m + R l_{(m+1)}}{2}$, and $R l_m = \frac{\Delta x_m}{\sigma_m^{eff}}$.

From Figure 3, it is obvious that instead of the potential in nodes, we can use the potential difference to obtain the currents. Thus, we can define new variables as follows:

$$\begin{cases} \Delta V s_m = \phi_{s(m+1)} - \phi_{sm} \\ \Delta V l_m = \phi_{l(m+1)} - \phi_{lm} \\ \Delta V J_m = \phi_{sm} - \phi_{lm} \end{cases} \tag{11}$$

Finally, in each volume, there are three unknowns (Eq. (10)) and three equations (i.e. Eqs. (4)-(6)) which can be solved to obtain the solution. To have a good accuracy, the whole battery is divided into a number of (namely n) volumes in series which will result a system of 3n unknowns and 3n equations (some of them neglected in the separator region). This model is illustrated in Figure 4. By solving this system of equations, the potentials in electrodes and electrolytes can be obtained.

## 2.2. *Step 2*

To obtain the other battery parameters, the species equations in Table 1 are solved numerically by Keller-Box method. To solve these equations, the potentials are taken form step 1 hence are not considered as unknowns. The Keller-Box method and its application to battery modeling is explained in [5] and is not mentioned here again. After obtaining the battery parameters in this time step, the whole procedure is repeated again to advance to the next time step.

## 3. Results and discussions

To verify the above mentioned procedure, the discharge problem of a flooded lead-acid battery has been simulated. Flooded lead-acid equations can be obtained by eliminating the gas evolution equations from the above system. This sample has been studied by Gu et al. [1] and reproduced by Esfahanian and Torabi. [5]. All the necessary parameters are the same as the ones used by Gu et al. [1]. Figure 5(a) shows the voltage variation of the cell vs. time. As it can be seen, the results of this method match the other results very well. Figure 5(b) shows the variation of acid concentration vs. time in different timesteps. The results show that this procedure is also capable to capture the variation of space distributed parameters as in CFD models. Furthermore, this method is about 200 times faster than pure CFD models.
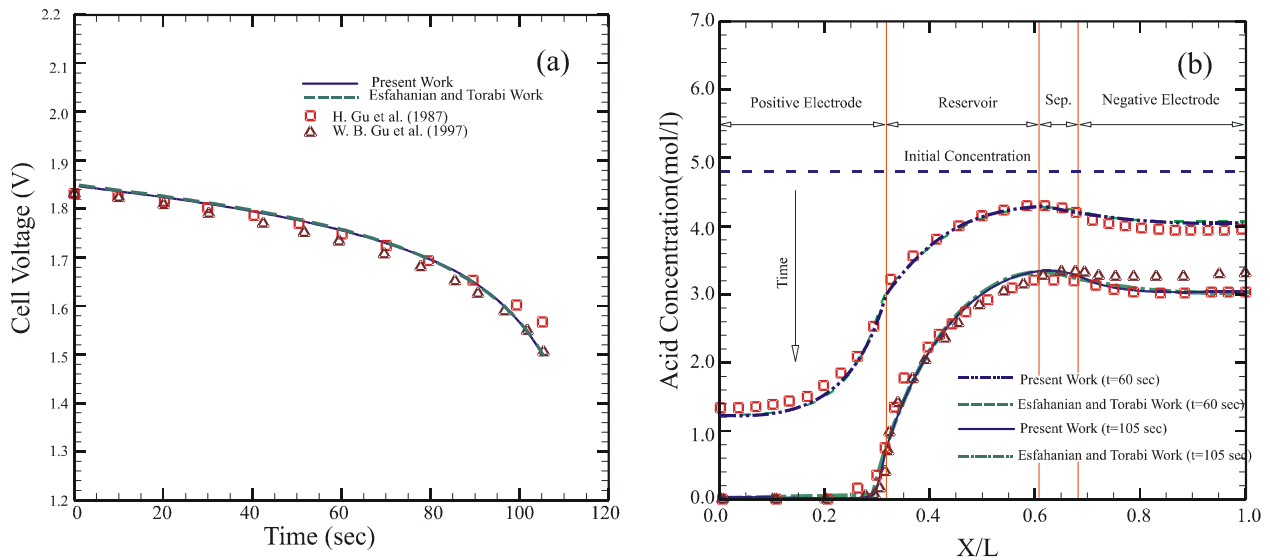
Figure 5: (a) Cell potential vs. time during discharge (b)Acid concentration distribution in cell

To investigate the effect of oxygen evolution in battery charging, a sample test is solved which was first introduced by Gu et al. [4]. Figure 6 shows the variation of cell voltage vs. time for charging. As it can be seen, at the end of charge, the voltage of the cell remains nearly constant while the oxygen cycle begins to develope. The deviation of the two numerical curves is due to the different values used for simulation.
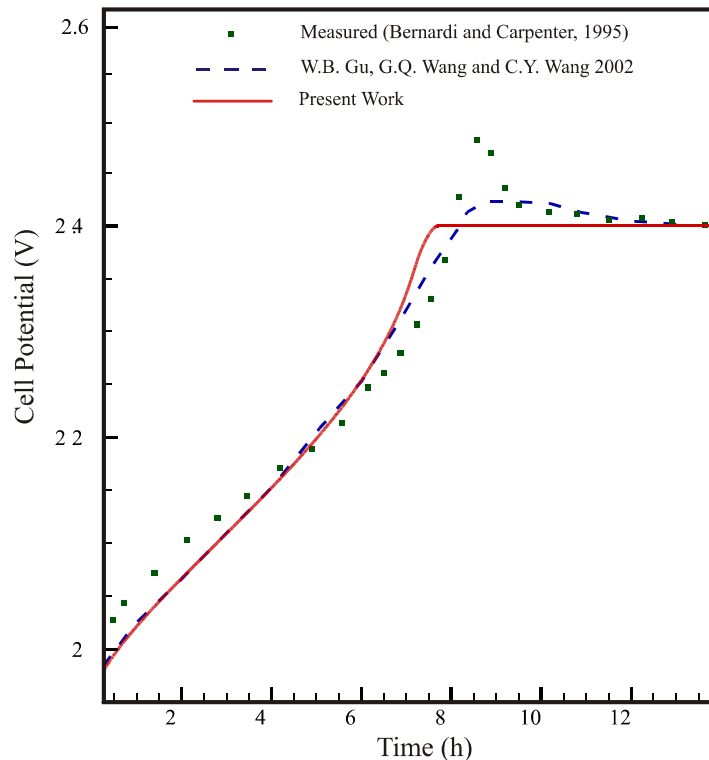


Figure 6: Cell potential vs. time during charge and overcharge.

In Figure 7, the solid and dashed curve show calculated cell voltage during constant current discharge, rest, charge and over charge of a battery with and without gas cycling, respectively. In the absence of oxygen cycling, the voltage rise very sharply at the end of charge (SOC=1). This happens because all the available $PbSO_4$ has been converted to either $Pb$ or $PbSO_4$ and since there
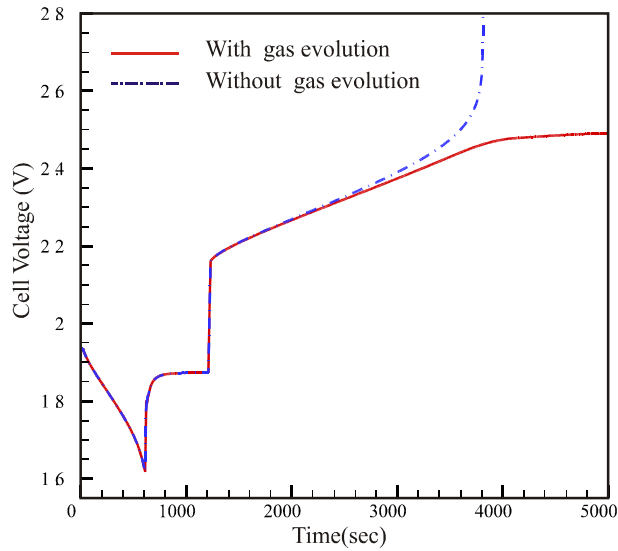
Figure 7: Cell potential vs. time during discharge,rest, charge and overcharge.
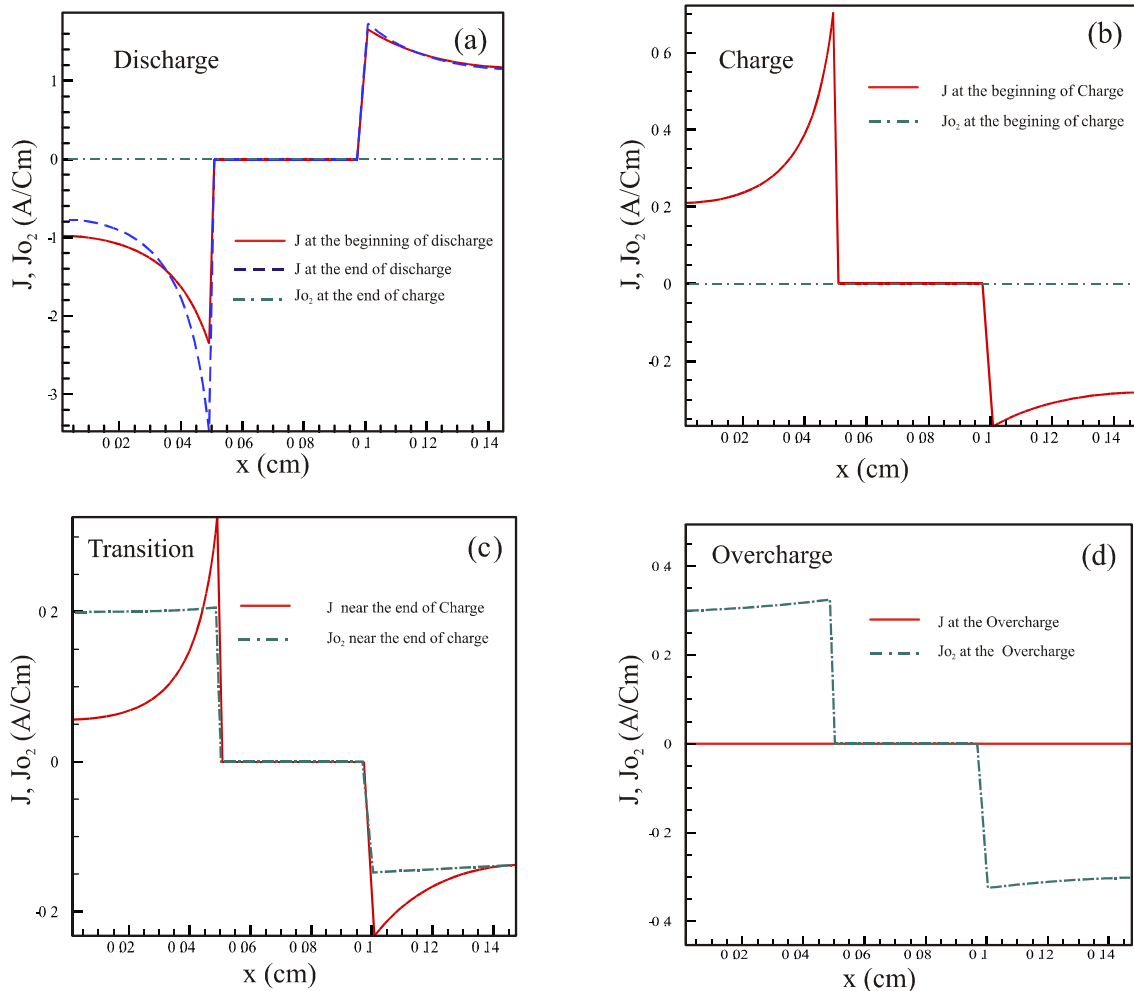


Figure 8: Distribution of J, $J_{O_2}$ during (a) Discharge, (b) Charge, (c) Transition and (d) Overcharge.

is no side reaction, a small amount of current causes a sharp jump in voltage. But in the presence of side reactions, the excess current goes into the oxygen cycle reactions and the battery voltage remains nearly constant.

Figure 8 shows the distribution of J and $Jo_2$ in the cell for different states of charges and discharges. According to Figure 8(a) and 8(b), the amount of $Jo_2$ can be neglected when the battery is discharging or charging, because the main reactions are more dominant than the others. Figure 8(c) shows that when the battery is near fully charged state, the main reactions rates are reduced while the secondary reactions occur intensively. Finally when the battery is fully charged, only secondary reactions are present and therefore, the current density is only due to side reactions.

## 4. Conclusions

In this paper an improved mathematical model for VRLA batteries based CFD and ECM has been introduced. This model inherits accuracy of CFD model and physical understanding of ECM. Moreover, it is very fast which makes it quite suitable for real-time simulations. The present model not only predicts battery dynamical characteristics but also unlike the classical ECM model, is capable to solve distributed parameters such as acid concentration distribution versus time. The present approach is verified by previous CFD models and experimental data. The results shows that this model has a good accuracy and the execution time is quite fast enough for real-time purposes.

## 5. Acknowledgment

## 6. References

[1]   J. Newman and W. Tiedmann, AIChE J., 21, 25 (1975).

[2]   D. M. Bernardi, H. Gu, and A. Y. Schoen, ibid., 140, 2250(1993).

[3]   C. Y. Wang, W. B. Gu, "Micro-Macroscopic Coupled Modeling of Batteries and Fuel Cells: I Model development," J. Electrochem. Soc. 145 (10) (1998) 3407-3417.

[4]   W.B Gu, GQ. Wang, C. Y. Wang, Modeling the overcharge process of VRLA batteries" J. Power Sources, 108 (2002) 174-184.

[5]   V. Esfahanian, F. Torabi, "Numerical Simulation of Lead-Acid Batteries using Keller-Box Method," J. Power Sources, 158 (2006) 949-952.

[6]   H. J. Bergveld, W. S. Kruijt, P. H. L Notten, *Battery Management Systems Design by Modeling*, Published by Kluwer Academic publishers, 2002

[7]   V. Esfahanian, F. Torabi, R. Afzali, "Engineering Simulation of Lead-acid Cell Characteristics and Processes in Batteries," 8th ISAEST Conference, India, 2006.